Martin, P., Connor, D., Payton, O., Leal Olloqui, M., Keatley, A., & Scott, T. (2018). Development and validation of a high-resolution mapping platform to aid in the public awareness of radiological hazards. *Journal of Radiological Protection*, *38*(1), [329]. https://doi.org/10.1088/1361-6498/aaa914

Development and validation of a high-resolution mapping platform to aid in the public awareness of radiological hazards

OPEN ACCESS
IOP Publishing | Society for Radiological Protection Journal of Radiological Protection
J. Radiol. Prot. **38** (2018) 329–342 (14pp) https://doi.org/10.1088/1361-6498/aaa914

Development and validation of a high-resolution mapping platform to aid in the public awareness of radiological hazards

Peter G Martin, Dean Connor, Oliver D Payton, Macarena Leal-Olloqui, Anya C Keatley and Thomas B Scott

Interface Analysis Centre, HH Wills Physics Laboratory, University of Bristol, BS8 1TL, United Kingdom

E-mail: peter.martin@bristol.ac.uk

Received 27 November 2017, revised 15 January 2018
Accepted for publication 19 January 2018
Published 15 February 2018

Abstract

The distribution, quantification and exposure-related effects of radiation in the environment, arising from both natural and anthropogenic sources, is of great (and growing) concern for global populations. Recent events at the Fukushima Daiichi Nuclear Plant (FDNPP) have further highlighted the importance of developing radiation mapping technologies that not only contribute to the continued assessment of contamination, but can serve as an educational tool for members of the public regarding both its behaviour and extent. With an even greater number of people possessing smart-phone technology, a light-weight and portable 'connected system' has been developed to demonstrate to users the calibrated radioactive dose rate in an area, viewable in real-time through a dedicated phone application. As well as allowing for system users to be alerted where variations in dose rate are experienced, the combined results from multiple systems are viewable through a custom-built desktop application—permitting the output obtained via any number of units to be similarly displayed in real-time. A successful initial trialling of the system is described at a former tin mine in Cornwall (south-west England)—known to exhibit low, but identifiable radiation anomalies in discrete areas. Additional applications outside of its educational usage are also discussed.

Supplementary material for this article is available online

Keywords: radiation mapping, legacy contamination, mining, education, radiation detection, Cornwall

(Some figures may appear in colour only in the online journal)

1. Introduction

As it cannot be smelt, seen or heard, and requires specialist detection equipment to be measured, ionising radiation has largely been viewed by the public as a highly-mysterious phenomenon and one for which it is difficult to easily understand its fundamental properties and the hazard it presents. Whilst being essential to life and the planet upon which we exist, it is the negative events such as the nuclear accidents at Chernobyl and Fukushima, alongside the large-scale weapons testing of the 1960s, for which radioactivity has become synonymous. In contrast, few people fully appreciate how radioactivity occurs naturally, and that considerable doses can be encountered as part of routine activities—despite national estimates and regulatory guidelines [1].

One of the UK's largest mapping projects undertaken to determine the spatial extent of naturally occurring radioactivity was performed by the British Geological Survey (BGS) as part of the 'Tellus South-West' Project [2]. As part of this extensive work, an airborne radiation survey was conducted over south-west England—a region known to exhibit elevated radioactivity associated with the large-scale intrusive igneous activity, which produced a series of regionally outcropping granite bodies [3]. The results, which are available publicly online, show significantly elevated (but highly localised) radioactivity across parts of the region, all of which are naturally occurring. Many areas identified in this work, however, detail dose rates comparable to large areas of Japan that are currently undergoing repopulation after having been formerly contaminated by the 2011 accident at the Fukushima Daiichi Nuclear Power Plant (FDNPP) [4].

It was following the magnitude (M_W) 9.1 earthquake, 15 m tsunami and subsequent release of vast quantities of radioactive material from Japan's FDNPP that an increased need to not only monitor radiation, but educate its citizens on its impact and true extent, was identified. An additional need to undertake rapid, high-resolution radiological surveying in the immediate aftermath of such an incident was further highlighted. Realising the absence of any such system, the not-for-profit, small ($15 \times 10 \times 5$ cm) Safecast bGeigie-nano device (cost $1500 USD fully-assembled) [5] was developed utilising specially constructed low-cost Geiger–Muller (GM) detector-based instruments transported by members of the public to obtain a calibrated dose-rate map surrounding the coastal nuclear plant. Another mobile system was subsequently developed by Ikuta *et al* (2012) [6], to monitor the Shimane Prefecture of Japan, using a large germanium (Ge) semiconductor-type detector, transported in the rear of a vehicle. This vehicular-based detector follows on from the earlier development of a similar platform by Sakamoto *et al* (2001) [7], who suspended a NaI(Tl) detector outwards from the rear of a vehicle in order to determine the extent of any on-road contamination. Similar work at KURRI (Kyoto University), led to the production of the KURAMA (and subsequent KURAMA-II) platform [8–10]. Unlike the Safecast mapping system—the KURAMA system featured a solid-state CsI detector, with its higher counting efficiency as well as the ability to yield full isotopic results from the incoming radiation. This briefcase-sized KURAMA unit was initially designed for installation within a vehicle—but was subsequently evolved for use through walking or transportation on a bike. Whilst the Safecast system is small and highly portable, it is unable to produce an isotopic spectrum of any

Table 1. Comparison of the features for currently available radiation detection and mapping platforms.

	Safecast	KURAMA I/II	NaI-CBS	Ge-CBS	University of Bristol (*this study)
Production date	2011	2013	2001	2012	2013
Detector type	GM	Scintillator	Scintillator	Semiconductor	Scintillator
Detector material	Gas: Ne + halogen	CsI(Tl)	NaI(Tl)	Ge	CsI(Tl)
Detector dimensions	5.4 cm (diameter) 1.3 cm (height)	13 × 13 × 20 mm (l × w × h)	5 cm spherical	8 cm (diameter) 9.2 cm (length)	2.5 × 2.5 × 5.1 cm (l × w × h)
Minimum limit of detection	NOT STATED	0.01 μSv/hr (^{137}Cs)	NOT STATED	5×10^{-5} μSv/hr (^{137}Cs)	0.01 μSv/hr (^{137}Cs)
System weight	0.65 kg	NOT STATED	NOT STATED	NOT STATED	0.5 kg
System dimensions	15 × 10 × 5 cm (l × w × h)	35 × 18 × 20 cm (l × w × h)	NOT STATED	NOT STATED	15 × 12 × 8 cm (l × w × h)
Transport mechanism	Personal/Vehicle	Vehicle	Vehicle/ Helicopter	Vehicle	Personal/Vehicle/UAV[b]
Control architecture	Microcontroller	CompactRIO[a]	Computer	Computer	Microcontroller
Reference	[5]	[9, 10, 24]	[7]	[6]	—

[a] a board combining a real-time controller, reconfigurable input-output modules (RIO), field programmable gate array module and an ethernet expansion.
[b]UAV—Unmanned Aerial Vehicle.

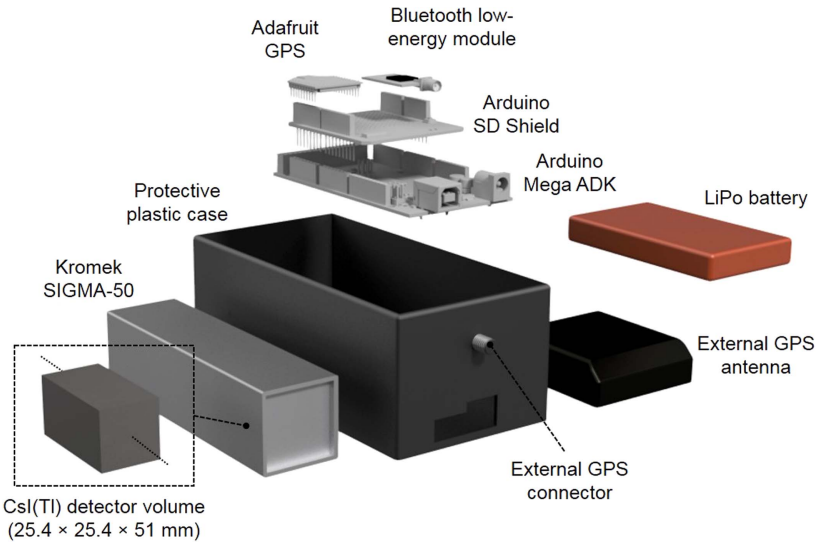

Figure 1. Graphical representation of the system electronics alongside a SIGMA-50 radiation detector.

radiological contamination. The KURAMA system on the other hand is considerably larger, with dimensions of 18 × 20 × 35 cm (outputting measurements recorded over the previous 3 s). A comparison of these ground-based detection and mapping options, is shown in table 1.

When compared, the system presented within this work (cost $2300 USD fully-assembled—without accompanying mobile phone), however, combines the advantages of both platforms, being both highly portable as well as fully-spectroscopic. Due to its size, the system could be deployed via any number of carrier methods, as well as on foot. The application of secured, Bluetooth low-energy data transmission between the detection/processing unit and the operator's wireless-enabled smart phone allows for centralised as well as individual visualisation of data in real-time—important not only with respect to planned radiological surveys, but more so as a powerful tool in educating those using the system on various aspects of radioactivity.

2. Materials and methods

2.1. Detection unit

A graphical rendering of the system electronics is shown in figure 1, consisting of the handheld gamma-ray radiation detector and external GPS antenna, both connected to an environmentally-sealed plastic enclosure containing the system processing, logging and transmission electronics. These electronics consist of a main Arduino ADK microcontroller board alongside SD-logging, Bluetooth low-energy (BLE) (RedBear Lab BLE shield) and GPS (Adafruit Ultimate GPS breakout/MTK3339) shields—all of which are powered through an onboard power distribution/regulation circuit, with LED indicators to confirm the system status. Whereas any number of USB-type detectors could be attached to and controlled by the platform's electronics (following modifications to the unit's software) the radiation detector employed in this work was a Kromek Ltd SIGMA-50 CsI(Tl) scintillator detector, with an active detection volume of 32.8 cm^3 [11].

As with the previously described systems (table 1), the components selected to produce this detection and mapping unit were chosen to keep production costs as low as possible—whilst still producing a rugged and powerful platform. As a result, the total cost of the system is comparable to that of the other systems ($2300 USD fully-assembled). The simplistic design of the system electronics, however, permits a variety of different radiation detectors to be used interchangeably with the platform—following a selection through the platform's internal control settings.

The detector has an energy range of 50 keV–1.5 MeV (across 4096 channels) with a maximum count rate of 5000 counts per second (CPS) and an energy resolution of $<7.2\%$ full width at half maximum at 662 keV. Photons incident onto the detector with energies greater than the detector's maximum (1.5 MeV) are processed. However, they are placed into the highest channel number (4096) of the detector. (*N.B. Despite this recording of* >1.5 MeV *gamma-ray photons within the highest energy bin, less than* $10^{-5}\%$ *of the total counts were in this channel*). To calibrate each detector and assess the gain drift over time, several different gamma-emitting radionuclides (Cs, Am, Co and Eu) were positioned in close proximity to the detector unit (in a laboratory setting), with the channel numbers corresponding to the various emission peaks used to derive a linear plot, and therefore determine an energy-per-channel value. As well as undertaking this energy calibration for each SIGMA-50 detector used in this study prior to its field deployment, to ensure this calibration had remained constant, a repetition was performed post-survey. From this replication, no change in the channel number for specific photon energies was recorded for any of the detectors used. As a consequence, the gain drift of the detector was determined to not represent a concern (*N.B. Year-long usage of the detector has shown no drift in the detector's energy-per-channel value*). However, post-processing of the data could permit any such drift to be eliminated. Consisting of a larger detector volume with inherently greater sensitivity than the previously used GR1 cadmium zinc telluride (CZT) gamma-spectrometer ($1 \times 1 \times 1$ cm) [12, 13], the $25.4 \times 25.4 \times 51$ mm CsI(TI) crystal (figure 1) is enclosed within a $35 \times 35 \times 130$ mm aluminium case, approximately 1 mm in thickness. This, despite existing with a stated spatial resolution of ± 3 m (as with any GPS module).

2.2. System software

Control of the detector and associated electronics is performed via software developed at the University of Bristol. Incoming data from the gamma-spectrometer is sampled at a frequency of 2 Hz by the microcontroller as a string of photon energies, incident onto the detector during the preceding 0.5 s. These energies were then paired alongside the geographical location of the unit, as determined via the systems onboard GPS module. These fully-spectroscopic and georeferenced data were then written in real-time to an onboard micro-SD card. Owing to the amount of data produced, alongside limitations that exist on the total volume of data capable of being carried over a radio frequency (RF) signal, it was not possible to wirelessly transmit full spectroscopic data. As a consequence, as well as being stored on the Arduino ADK microcontroller as a data-array for later reconstructing a full gamma-ray spectra, only the value for the CPS (number of detection events in the 0.5 s sampling window x2) as determined at each location point, was transmitted in near real-time (500 ms delay) via an encrypted RF data stream back to a remote base station (a computer running additional software developed at the University of Bristol) using an XBee (Digi International Inc.) 802.15.4 Point-to-Point RF Module. To enable the radiological intensity data to be displayed on the accompanying smart phone wirelessly tethered to the unit, the same CPS and location data were additionally transmitted using an encrypted BLE signal. In each instance, either or

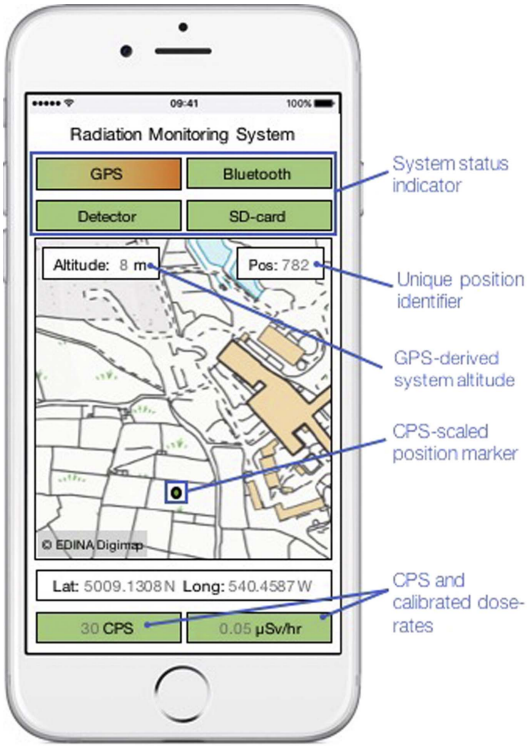

Figure 2. Screenshot of the iOS application developed to display survey results on the operator's smart phone.

both wireless signals could be switched off—depending on the system's desired usage and operational environment. The operational lifetime of the system, however, was not adversely affected by the transmission of both wireless (RF and BLE) signals. Whereby, through the use of a standard 2500 mAh lithium polymer (LiPo) battery, data could be collected (and transmitted) for a 12 h period without the need to replace the system's battery. An indication of the device's battery status is provided through the phone-base application linked to the unit.

2.3. Smart-phone application

A screenshot of the iOS application, developed for displaying the status of the device in addition to the progress/results of the radiological survey, is shown in figure 2. To aid the user in ensuring that the system is functioning correctly, a series of labelled status indicators are shown at the top of the application screen—with green representing correct function, and orange/red illustrating an error, or that the system is still preparing. Below these indicators is a user-scrollable map, with the GPS-derived location of the unit shown as a colour-scaled position marker (the colours of which are defined by the user). At the base of the application screen is displayed both the latitude and longitude of the system (as decimal degrees) in addition to raw CPS value and a calibrated value for the dose rate (detailed in section 2.5)—specific for each detector attached to the system. This calibration constant is applied within the application settings.

To streamline the amount of data transmitted via either Bluetooth or RF, no spectroscopic data are relayed wirelessly—with only a value for the total (gross) CPS being sent to either base unit (computer or phone). In contrast to the data transmitted via traditional RF telemetry to the main base station—which was displayed in its entirety within the software, the iOS application, however, depicted only the most recent data point received from the accompanying detection unit, hence preventing large volumes of data being stored on the user's device. A unique position identifier, shown on the top right of the map could be used to later reference any points of interest within the main analysis software. This smart-phone visualisation was selected, with the results serving as both a reference for the operator (to detail ground that had been covered) and also as an informative tool to detail site-wide radiation differences.

2.4. Survey site

As an initial site to test the application of multiple detection systems, the Geevor Tin Mine in Cornwall, south-west England, was chosen. The coastal site, like many others located across the region, ceased operations in the late twentieth century due to ever-increasing competition from overseas imports. Identical to many other historical small-scale tin and copper mining operations synonymous with the area, after ore extraction, subsequent processing was undertaken on-site—with the production of considerable quantities of radiologically contaminated spoil, stored as extensive waste heaps. Viewed as an important cultural asset detailing the region's vast former industry, the Geevor site is now a popular visitor attraction. Whereas these waste heaps have been removed and the site remodelled in the almost thirty years since its closure, there still likely exist isolated areas where low levels of radiological contamination are anticipated to occur.

2.5. System calibration

To ensure consistency between the different SIGMA-50 detector systems used during this work, a series of calibrations (both in-lab or field-based) were performed. Owing to the cuboid shape ($25.4 \times 25.4 \times 51$ mm) of the CsI(Tl) detector crystal contained within the SIGMA-50 unit, a quantification of the influence of its orientation was undertaken. The results of exposing three identical detectors to different radiation fields (intensity and orientation from front face) are shown in figure S1 and is available online at stacks.iop.org/JRP/38/329/mmedia. Apparent is the considerable CPS variation experienced with differences in its orientation—as a result, a consistent positioning of the device—with the system's long-axis parallel to the ground, which was used to attain maximum system sensitivity at only a marginal degradation to the crystal's stopping power [14].

In contrast to the formerly used CZT composition Kromek GR1 gamma-ray spectrometer, where an exponential (logarithmic) decrease in detector efficiency with increasing photon energy was determined [15] (reducing to 0.005% detection efficiency at 1500 keV), the CsI-based SIGMA-50 is characterised by an improved detector efficiency at higher incident photon energies (0.2% detection efficiency at 1500 keV) [16]. Through applying the approximately linear reduction in detection efficiency that is derived (when graphed onto a log-linear scaling), a compensation for this energy dependence/efficiency of the detector, can be accounted for. This correction is performed digitally on either the mobile phone or base-station platform, whereby the mathematically derived function describing the trend is applied to correct for such detector inefficiencies.

After applying this correction to the SIMGA-50 derived CPS data to correct for such an intrinsic inefficiency, a calibration to permit the conversion from CPS to a meaningful value of dose rate (μSv/hr) was undertaken—the results of which are shown in figure S2 (plotted from all three units). Also performed within the laboratory, a calibrated RADEX dosimeter was additionally exposed to the same incident radiation fields as described previously for the orientation calibration presented in figure S1. A strongly linear relationship between both units was observed from this comparison.

An additional inter-system comparison was undertaken within the field to analyse the impact of differences in orientation (survey direction) at which ground-based monitoring is undertaken, as well as the influence of human (bodily) attenuation upon the results. As has been quantified in earlier studies [17, 18], a reduction in the maximum recorded intensity of between 20% and 30% has been attributed to the radiation shielding imposed by human interception and absorption of gamma-rays. Using a location at the site known to exhibit elevated levels of radioactivity, three different operators were asked to walk around this point as if conducting a routine survey—following a closely-spaced (0.5 m grid separation) raster path-line around the radioactive source. A plot detailing the radiation intensity (as CPS) against the GPS-derived distance from that point is shown in figure S3. A linear decline in radiation intensity is observed. Whilst an inverse-square ($1/\text{distance}^2$) relationship would be typical of such a scenario, the small emitter-detector distances associated with these measurements, combined with the non-point geometry of the source utilised, therefore provide mechanisms to account for such a relationship. A degree of variation, amounting to a difference of up to 31% (average = 23%), is seen at specific distances from the source (viewed as the vertical spread of data)—which is consistent within the typical reductions in intensity defined by the earlier works, due to the interception and absorption of gamma-rays by a human surveyor.

An accuracy assessment of the Adafruit Ultimate GPS module used in this work comprised the final portion of the pre-survey system calibration. To undertake this assessment, the position of a series of locations across the site was determined using a Leica GNSS dGPS unit, with the same geospatial positions subsequently determined using the Adafruit Ultimate GPS module. The results of this inter-system calibration exercise are shown in figure S4. A mean offset between both units of $\pm$0.43 m was determined from this study, hence, sub-metre spatial resolution of the system was attainable.

3. Results

With the primary goal of this work being to develop an integrated platform for radiation mapping that also allowed for the simultaneous education of its users to potential radiological hazards—the complete radiation map of the site, as determined through the application of three simultaneously operated units, is shown in figure 3. An accompanying Ordnance Survey map detailing the dose rates at many positions across the site for inter-system comparison/calibration of results is shown in figure 4, determined using the RADEX handheld survey meter. Despite elevated, yet highly-isolated levels of contamination existing at portions of the Geevor Site (shown in red); the levels of radiation are low—as would be expected for a mining site that has undergone extensive site-wide remedial activity. The average dose rate recorded by the system across the entire site during this work was 0.35 μSv/hr, marginally higher than the UK average background rate of 0.31 μSv/hr, yet more than half the 0.79 μSv/hr average radiation exposure received by those residing within Cornwall (mostly due to radon gas exposure) [1].

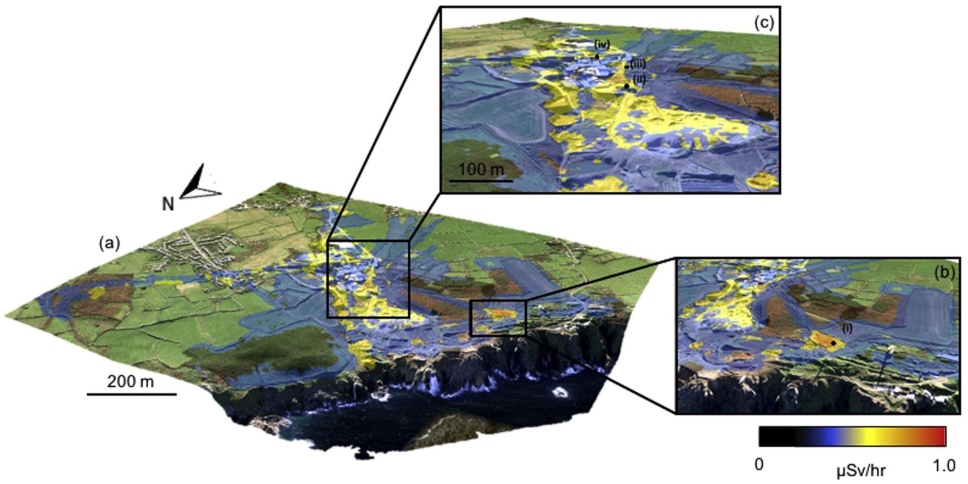

Figure 3. 3D post-processed rendering of the radiation mapping survey at the Geevor Site, showing; (a) full site area, (b) locality (i), and (c) localities (ii to iv). Each of the four locations is associated with former operations at the site.

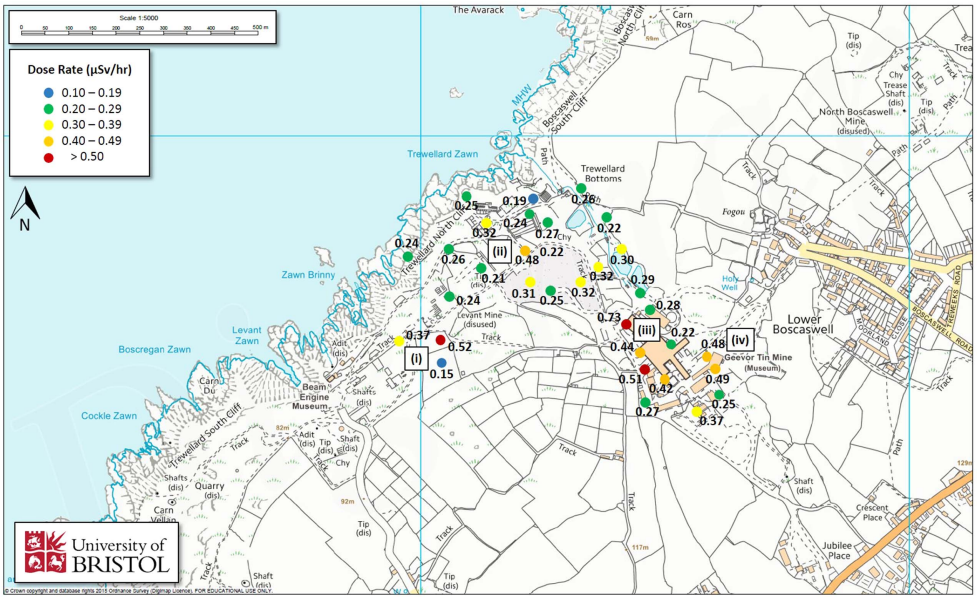

Figure 4. Dose-rate measurements obtained at distributed locations around the site, obtained using the RADEX handheld dosimeter. The positions ((i) to (iv)) represent the same locations as indentified in figure 3 and the gamma-ray spectra shown in figure S5 (base map © Ordnance Survey 2016).

Owing to the real-time feedback to the operator's tethered iOS mobile device, a high level of ground coverage attainable by each of the detection and mapping systems is observed. Depicted within the results is; (a) the units together covering a large area of the Geevor site in 6 h, but most-significantly, (b) evaluating this through a series of tightly-spaced

survey grids. This, combined with the rapid readout rate of the system, permits sub-metre coverage and removes the requirement to perform inter-point smoothing and infilling that would otherwise be required between widely-spaced data points—hence degrading the ultimate spatial resolution attainable.

Observed within the radiation map of the entire site presented in figure 3(a), and as expected given the location and nature of works on the site, is the prominent area of elevated dose rates across the central, downwards sloping portion of the site—the location of the site's former mining and processing operations. The areas bordering this portion of the site all exhibit uniform, low levels of radioactivity with dose rates of 0.15–0.29 μSv/hr (typical of a low UK background level). Unlike these low dose-rate areas (found at level and slightly elevated positions to the west and east of the primary southwards trending contamination 'plume'), the central band of elevated radioactivity is associated with the exposure of bare ground, where there was no considerable thickness of grass, bracken and soil—having been stripped away during earlier remedial operations. Not only do soil and vegetation layers provide a blanketing means of attenuating the emission of gamma-rays from the underlying rock strata, they provide a binding and stabilising effect on any sloped ground. Based on the recorded data, the stability of the bare slopes is inferred to have been reduced and hence the radiological data imply that a downslope migration of mineral-derived radiological contamination has occurred.

One of the highest observed radiation levels at the site, identified as position (i) in figure 3(b), is not associated with the central site operations or even a building on the site—located, however, 400 m to its north-west. This flat 50 $\times$ 50 m area consisted of a former spoil heap that has since been levelled, with the region constituted by a thick red mud following bulk material removal and land reshaping. It is highly likely also, that material deposited at this locality was sourced additionally from the neighbouring Levant Mine—a site similarly extracting copper and tin during the nineteenth century. A dose rate measured for this locale is 50% greater than the site-wide average for the entire Geevor site, at 0.50 μSv/hr. This location is distinct from the other 'hot-spots' of elevated activity recorded at the Geevor site, owing to its large lateral extent—rather than being highly localised.

As expected, elevated yet highly localised (metre-scale) regions of radioactivity are associated with positions on the site where both mining and the subsequent processing of the extracted (ore and gangue) material occurred. Identified as points (ii), (iii) and (iv) on figure 3(c), located within the sloping area of the general elevated radioactivity formerly described (and shown graphically in figure 3(a)), are three distinct points. The northern-most of these three sub-localities is the largest in its extent as well as showing the greatest activity of the entire Geevor site. At approximately 50 m in extent and with dose rates of 0.72 μSv/hr, the activity from position (ii), as with (i) further to the north, is witnessed to also originate from a region of un-remediated land—left as a legacy tip from former operations. A portion of this contamination is also associated with the corner of a neighbouring building that now houses the gold-panning exhibition—with a large collection of original wooden settling tables used to separate the valuable ore from the associated gangue species.

Thirty-five metres south-south-east of this large and higher-activity anomaly exists location (iii) (figure 3(c)). Not as spatially extensive or as radiologically active as locality (ii), the position of this 'hot-spot' occurs at the location of a number of large granitic boulders—forming part of an exhibition outside the museums entrance. This region of enhanced activity is the most spatially limited of all the localities, at less than 5 m in extent. Whilst minimal in size—of note, however, is the dose rate that this entirely natural material exhibits—at 0.50 μSv/hr, identical to (i)—where spoil generated from this material was deposited across a considerable area of the site.

The final point showing elevated activity above the general background, located 50 m south-east of locality (iii), is the anomaly marked as (iv) in figure 3(c). Of all the four points identified through this high-resolution gamma-spectrometry survey, this body displays the lowest recorded dose rate at only 0.46 μSv/hr; only marginally above the site-wide background level. As with the other localities (i), (ii) and (iii) before it, this locality represents the location of former activities on the site—in this instance the mine's main 'Victory Shaft' tower and the neighbouring museum reception building, where assorted scrap metal (formerly part of the mine's construction) is located.

When the results derived using this newly developed mobile survey platform are directly compared with the numerous point measurements collected over the same area via the handheld RADEX unit, a high level of consistency between the measurements is observed. As can be seen in figure 4, not only is the location of these anomalies identified, but the magnitude of the activity (dose rate), alongside the spatial extent of the contamination. Owing to the way the data are acquired during the survey (as a series of calibrated channel energies) and subsequently stored—a gamma-ray spectrum can be derived from the results—permitting the forensic attribution of specific radionuclides to the contamination. The gamma-ray spectra acquired at the four anomaly sites (i to iv) in figures 3(b) and (c) are shown in figure S5. As expected for a series of spectra derived from a common uranium-ore source, the recorded emission peaks are identical and result from the radioactive decay of the gamma-emitting daughter products that have subsequently ingrown since the minerals were emplaced into the country rock—with the peaks identified in figure S5 occurring from the radioactive decay of ^{214}Bi and ^{214}Pb. A close similarity in the relative intensities (detector efficiency corrected) of the contributing peaks ($\pm$4%) between each of the spectra implies; (a) a commonality to the source material and (b) secular equilibrium in the radioactive ore minerals—hence suggesting that neither preferential transport, nor biological uptake, has occurred.

4. Discussion

Over a total of 18 man hours, 70 000 m of survey length was mapped with the results from the three mobile units viewed in real-time by both the system's on-the-ground operator as well as remotely, via a secure RF transmission of the data. From each of the mapping units, a number of regions showing elevated activity levels were observed. However, whilst the recorded intensity was notably greater than the land that surrounds them—each of these anomalies represents a dose rate that is well below background radiation levels typical of Cornwall as well as being highly localised in their spatial extent—some of which are sub-metre in size.

The ability of the on-the-ground operator to see in real-time the subtle variations in radioactivity means that surveys can be conducted more intuitively, with greater amounts of time, ground coverage and scrutiny dedicated to 'interest' areas. The real-time identification of discreet 'hot-spots' during the survey presented here, enabled the survey teams to return to these locations during the period of the survey to collect fixed point gamma-ray spectra, where photon counting was conducted for discrete (10–20 min) periods.

In addition to its use in routine monitoring, the platform also has the potential to be adopted as one of the toolkit technologies that would be required in response to a nuclear emergency. It is well documented that after the FDNPP accident, there was a lack of detailed knowledge for up to 2 weeks, as to the spread and intensity of ground-deposited radiation [19, 20]. This lack of knowledge led to initial decisions regarding evacuation of civilian populations in the nearby area to be overly risk averse, resulting in the forced relocation of some 162 700 people. The results of a recent statistical 'J-value' study by Thomas *et al* [21]

has indicated that under the Japanese Government's 20 mSv yr^{-1} safe-return criterion, it was not advisable to relocate any of the 162 700 people that inhabited the nearby towns and villages. This is because the inhabitants' calculated gain in life expectancy, even in the most contaminated settlements, would have been insufficient to balance the fall in their life quality index caused by their notional 'payment' of the costs of relocation (financial, physical and mental).

If a technology to rapidly determine the spread and intensity of the radiation had been available at the time of the Fukushima event, then perhaps different decisions would have been made about evacuation. Certainly, there is a well-stated requirement for the nuclear industry to improve the emergency response capability for any future nuclear emergencies [22, 23].

The systems presented here, have demonstrated the capability to rapidly record high sensitivity, metre-resolution data that is transmitted (securely) in real-time to a central (off-site) location. Not only does this enable the on-the-ground operators to understand their personal risk, but enables strategic decision makers (emergency response co-ordinators), working from a protected centralised location, to achieve a rapid analysis and assessment of the developing situation and thereby aid critical decisions to manage the situation.

Finally, when presenting radiation data to a scientific audience, it is wholly acceptable to use SI units of radiation dose and to expect an implicit understanding of the true risks posed by radiation, based on the intensity of the exposure. An equally implicit understanding is that radiation is ubiquitous.

5. Conclusions and future work

With real-time feedback combined with the operator's natural curiosity and desire to identify areas with the greatest radioactivity within an area, the application-based radiation mapping platform developed in this work has enabled a methodical survey of the former Geevor Tin Mine to be undertaken, with metre-scale areas of elevated radioactivity identified and spectrally characterised.

Whilst only one RADEX dosimeter was used opposed to the three of the newly-devised mobile phone-tethered radiation logging units, as can be seen from the volume of data collected from across the site, the fully autonomous collection of data by this new system permits 100s of times the data to be acquired over the same collection period (sampling data every 0.5 s). In addition to geospatially guiding operatives during surveys, the simplistic front-facing phone application allows for untrained personnel with no technical knowledge to use the platform whilst rapidly recording meaningful data. In addition to the initial usage of the system described here, however, the platform also has the potential to be deployed as part of an emergency response scenario—where results are required to be rapidly (and securely) transmitted to a central system to enable rapid analysis and an associated response.

Although already highly visual, and a powerful means with which to visualise zones of elevated radioactivity with respect to naturally occurring background levels, a number of improvements and enhancements to the system are planned. These modifications include:

- A graphical representation of dose rate (in addition to units of μSv/hr) to permit a *layman's* visualisation of radiation levels. This is proposed to take the form of an average hourly dose rate—with other possible correlations presented to everyday radiological exposures, such as proportions of a chest x-ray or hours spent on a transatlantic flight.

- Addition of a 'simplified' menu screen—displaying only limited information. Such a screen would remove the map, comprising the system's nine status indicators and data readouts.
- Streamlining of the data readout from the system, thereby giving the application's user the option (if desired) to view a fully-labelled gamma-ray spectrum of the incident radiation.
- The ability to use alternate base maps within the application, other than current OS plots. These could include both current and past satellite imagery maps as well as historical site maps.

Acknowledgments

The authors wish to acknowledge the financial support for this work provided by the Engineering and Physical Sciences Research Council (Ref: EP/K503824/1). Gratitude is also extended to the Level 3 Earth Sciences students at the University of Bristol who aided in the collection of the data for this work as well as to Mr P Savage and Mr M Simpson at Geevor Mine for their support in the work performed.

The data used in this work is freely available from the Mendeley Data Repository, doi:10.17632/jnp4t4bpgc.2.

ORCID iDs

Peter G Martin https://orcid.org/0000-0003-3395-8656

References

[1] Public Health England, Guidance: Ionising radiation—dose comparison. (https://gov.uk/government/publications/ionising-radiation-dose-comparisons/ionising-radiation-dose-comparisons). Date accessed: 13.01.2017
[2] Beamish D 2014 Environmental radioactivity in the UK: the airborne geophysical view of dose rate estimates *J. Environ. Radioact.* **138** 249–63
[3] Dines H G 1956 The metalliferous mining region of South-West England (London: HMSO)
[4] METI, Areas to which Evacuation Orders have been issued. (http://meti.go.jp/english/earthquake/nuclear/roadmap/pdf/150905MapOfAreas.pdf). Date accessed: 13.05.2016
[5] Safecast, About Safecast. (http://blog.safecast.org/about/). Date accessed: 24.10.2016
[6] Ikuta M, Gobara H, Tanaka A and Kimura K 2012 Car-Borne Survey Using Ge Semiconductor Detector in the Chugoku Region of Japan *Jpn. J. Health Phys.* **47** 198–203
[7] Sakamoto R, Saito K, Tsutsumi M and Nagaoka T 2001 Study on the measurements and evaluation of environmental external exposure after a nuclear accident, Hoken Butsuri.(http://iaea.org/inis/collection/NCLCollectionStore/_Public/33/009/33009956.pdf). Date accessed: 28.05.2017
[8] Andoh M *et al* 2015 Measurement of air dose rates over a wide area around the Fukushima Daiichi Nuclear Power Plant through a series of car-borne surveys *J. Environ. Radioact.* **139** 266–80
[9] Tsuda S *et al* 2013 Construction of a car-borne survey system for measurement of dose rates in air. KURAMA-II, and its application *JAEA Technology* **2013–037** 68
[10] Tsuda S, Yoshida T, Tsutsumi M and Saito K 2015 Characteristics and verification of a car-borne survey system for dose rates in air: KURAMA-II *J. Environ. Radioact.* **139** 260–5
[11] Kromek Group PLC, SIGMA Spec Sheet; Revision 6, (2015) 2 (http://kromek.com/downloads/sigma_rev6web.pdf). Date accessed: 23.06.2015

[12] Martin P G, Payton O D, Yamashiki Y, Richards D A and Scott T B 2016 High-resolution radiation mapping to investigate FDNPP derived contaminant migration *J. Environ. Radioact.* **164** 26–35
[13] Martin P G, Payton O D, Fardoulis J S, Richards D A and Scott T B 2015 The use of unmanned aerial systems for the mapping of legacy uranium mines *J. Environ. Radioact.* **143** 135–40
[14] Grodstein G W 1957 X-ray attenuation coefficients from 100 keV to 100 MeV *National Bureau of Standards Circular* **583** 13–50
[15] National Physical Laboratory 2013 Intrinsic Photopeak Detection Efficiency as a Function of Energy: Kromek GR1
[16] Bell S 2016 A comparison of emerging gamma detector technologies for airborne radiation monitoring *ANSRI 2016 (Dublin, Ireland, 11–13 May)* (National Physical Laboratory) http://spacescience.ie/ansri2016/ansri2016_talks/31-VI-Bell.pdf
[17] Jones H E and Cunningham J R 1983 *Physics of Radiology* Fourth Edition4th edn (Illinois, USA: Thomas Publishing, Springfield)
[18] Buchanan E, Cresswell A J, Seitz B and Sanderson D C W 2016 Operator related attenuation effects in radiometric surveys *Radiat. Meas.* **86** 24–31
[19] MEXT and US Department of Energy 2011 Results of the Airborne Monitoring by the Ministry of Education, Culture, Sports, Science and Technology and the U.S. Department of Energy. 6th May 2011 (http://radioactivity.nsr.go.jp/en/contents/1000/294/24/PressR04 0802 s.pdf). Date accessed: 14.08.2015
[20] NRA, Comprehensive Radiation Monitoring Plan, Tokyo, 2011. (http://radioactivity.nsr.go.jp/en/contents/8000/7758/view.html). Date accessed: 03.08.2017
[21] Waddington I, Thomas P J, Taylor R H and Vaughan G J 2017 J-value assessment of relocation measures following the nuclear power plant accidents at Chernobyl and Fukushima Daiichi *Process Safety and Environmental Protection* **112** 16–49
[22] Ashley S F, Vaughan G J, Nuttall W J and Thomas P J 2017 Considerations in relation to off-site emergency procedures and response for nuclear accidents *Process Safety and Environmental Protection* **112** 77–95
[23] Thomas P J 2017 Quantitative guidance on how best to respond to a big nuclear accident *Process Safety and Environmental Protection* **112** 4–15
[24] Hamamatsu Photonics K.K., Hamamatsu C12137-Series Specification, Hamamatsu City, 2017. (http://hamamatsu.com/us/en/product/alpha/R/4134/index.html). Date accessed: 06.09.2017